THE JOURNAL OF PHYSICAL CHEMISTRY Letters

Letter

Cite This: J. Phys. Chem. Lett. 2019, 10, 6274−6280

pubs.acs.org/JPCL

Mesoscale Organization and Dynamics in Binary Ionic Liquid Mixtures

Tyler Cosby,[†] Utkarsh Kapoor,[‡] Jindal K. Shah,*[,‡] and Joshua Sangoro*[,†]

[†]Department of Chemical and Biomolecular Engineering, University of Tennessee, Knoxville, Tennessee 37996, United States

[‡]School of Chemical Engineering, Oklahoma State University, Stillwater, Oklahoma 74078, United States

Supporting Information

ABSTRACT: The impact of mesoscale organization on dynamics and ion transport in binary ionic liquid mixtures is investigated by broad-band dielectric spectroscopy, dynamic-mechanical spectroscopy, X-ray scattering, and molecular dynamics simulations. The mixtures are found to form distinct liquids with macroscopic properties that significantly deviate from weighted contributions of the neat components. For instance, it is shown that the mesoscale morphologies in ionic liquids can be tuned by mixing to enhance the static dielectric permittivity of the resulting liquid by as high as 100% relative to the neat ionic liquid components. This enhancement is attributed to the intricate role of interfacial dynamics associated with the changes in the mesoscopic aggregate morphologies in these systems. These results demonstrate the potential to design the physicochemical properties of ionic liquids through control of solvophobic aggregation.

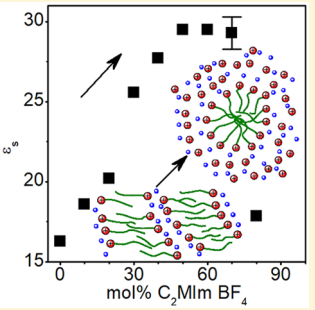

Downloaded via UNIV OF TENNESSEE KNOXVILLE on October 5, 2019 at 05:12:30 (UTC).
See https://pubs.acs.org/sharingguidelines for options on how to legitimately share published articles.

Elucidating the influence of mesoscale organization on the dynamics and transport properties of ionic liquids is critical to developing design criteria for their applications in chemical synthesis, nanoparticle growth, biomass processing, batteries, solar cells, and supercapacitors.[1−10] In the past decade, the formation of mesoscale polar and nonpolar domains in ionic liquids with substantial nonpolar, alkyl side groups was recognized in detailed X-ray scattering, neutron scattering, and molecular dynamics (MD) simulation studies.[11−16] Mesoscale organization has been used to qualitatively explain numerous experimental findings that imply spatially and temporally distinct regions within bulk ionic liquids.[11,17−26] Recent studies suggest that the existence and dynamics of the aggregates in neat ionic liquids, associated with fluctuations of the polar and nonpolar regions, correlate strongly with many of the physicochemical properties of ionic liquids, including transport properties such as zero-shear viscosity, dc ionic conductivity, and static dielectric permittivity.[27−32] However, no efforts to exploit the mesoscale organization to design novel ionic liquids with unique physical and chemical properties have been reported. In this work, it is demonstrated that by mixing ionic liquids with varying degrees of solvophobic aggregation it is feasible to design distinct liquids with macroscopic properties that significantly deviate from weighted contributions of the neat components.

The local organization, or morphology, of the mesoscale aggregates is in part determined by the relative volume fractions of the polar and nonpolar groups of the component ions.[11] In amphiphilic imidazolium, pyrrolidinium, piperidinium, quaternary phosphonium, and quaternary ammonium ionic liquids, increasing the alkyl chain length on the cation head group tends to swell the nonpolar domain, leading to a progression from globular morphology to a loosely defined bicontinuous morphology with percolating polar and nonpolar domains.[13,14,33,34] Conversely, at a given length of the alkyl chain on the cation, the polar domain may be enlarged (or reduced) by selecting an anion with a larger (or smaller) molar volume.[11] An alternative approach to altering the polar and nonpolar volume fractions is to consider mixtures of two or more ionic liquids with differing chemical structures.[29] Totally unexplored is the influence of composition-dependent morphology and the accompanying mesoscale aggregate dynamics on the physical and chemical properties of ionic liquid mixtures.

In this study, we highlight an approach in which complementary experimental and computational techniques are employed to investigate changes to mesoscale aggregate morphology and dynamics as a function of composition in binary mixtures of the ionic liquids 1-octyl-3-methylimidazolium tetrafluoroborate (C_8MImBF_4) and 1-ethyl-3-methylimidazolium tetrafluoroborate (C_2MImBF_4). By mixing these two imidazolium ILs, which differ only in the cationic alkyl chain length, the bicontinuous morphology of neat C_8MImBF_4 is transformed to more isolated and spherical nonpolar aggregates, as indicated by X-ray scattering and MD simulations. As a result of the composition-dependent evolution in morphology, the mesoscale aggregate dynamics, as probed by dynamic-mechanical and broad-band dielectric spectroscopy, are significantly altered. The changes to aggregate morphology and dynamics result in a 100% increase in the static dielectric permittivity, also known as the dielectric constant, relative to that of either pure component.

Received: August 23, 2019
Accepted: September 27, 2019
Published: September 27, 2019

© XXXX American Chemical Society

DOI: 10.1021/acs.jpclett.9b02478
J. Phys. Chem. Lett. 2019, 10, 6274−6280

The chemical structures of C_8MImBF_4 and C_2MImBF_4 were chosen to approximate a mixture consisting of one amphiphilic and one predominantly polar ionic liquid. The imidazolium head group and the anion of each ionic liquid are identical in order to minimize the potential influence of mixture composition on the ion−ion interactions within the polar domains and at polar/nonpolar interfaces. In this way, the influence of mesoscale aggregate morphology and dynamics on the transport properties may be investigated independent of any change in ion−ion interactions. To probe the influence of composition on the mesoscale aggregate morphology and to verify the location of C_2MImBF_4 within the polar domain, neat C_8MImBF_4, neat C_2MImBF_4, and 30, 50, and 70 mol % C_2MImBF_4 mixtures were investigated by X-ray scattering and MD simulations.

The structure factors, $S(q)$, of the neat ionic liquids C_8MImBF_4 and C_2MImBF_4 and the 30, 50, and 70 mol % C_2MImBF_4 mixtures obtained at room temperature by small- and wide-angle X-ray scattering are presented in Figure 1a.

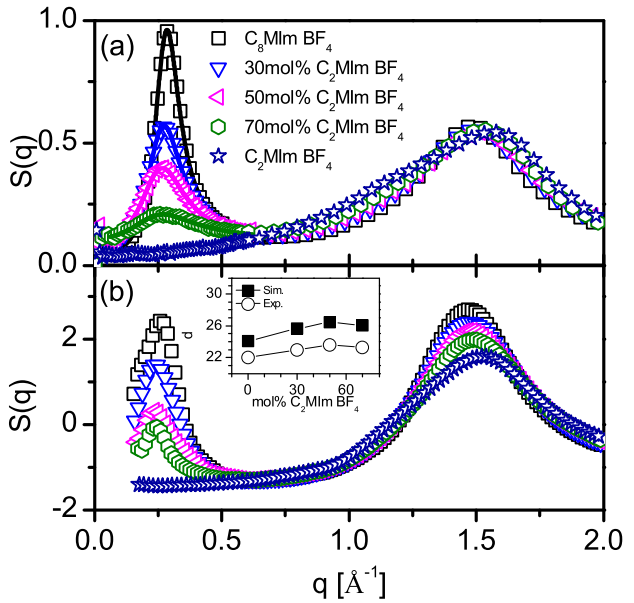

Figure 1. (a) Structure factors, $S(q)$, obtained by X-ray scattering. Lines correspond to fits with the Teubner−Strey model.[35] (b) Structure factors computed by MD trajectories. Inset: Comparison of the real-space correlation distance, $d = 2\pi/q_{max}$, of the prepeak obtained by simulation (sim.) and experiment (exp.).

C_8MImBF_4exhibits a prepeak at $q = 0.28$ Å^{-1} typical of self-assembled ionic liquids and assigned to the scattering from polar domains separated by a nonpolar domain.[11,17] With increasing concentration of C_2MImBF_4, the prepeak is reduced in intensity and shifts to slightly lower q values. The prepeak is well-described by the generalized Teubner−Strey model, developed to model the contribution of density fluctuations in bicontinuous microemulsions.[35−37] The obtained fit parameters (see the Supporting Information) are in close agreement with a recent work by Bruce and co-workers in which the evolution of morphology in a series of mixtures consisting of $C_{12}MIm\ NTf_2$ and $C_2MIm\ NTf_2$ was investigated by small-angle X-ray and neutron scattering coupled with MD simulations.[37] They reported a disruption of the bicontinuous morphology and a transition to more isolated prolate spheroidal aggregates upon dilution with $C_2MIm\ NTf_2$ The overall similarity between the two IL systems and the experimental results suggests that a similar transition in morphology occurs in the C_2MImBF_4/C_8MImBF_4 mixtures.

Further insight into the structural changes that alter the position and intensity of the prepeak is provided by MD simulations. Details of the structure factors calculated from the MD simulations may be found in the Supporting Information. The structure factors, shown in Figure 1b, reproduce the positions and relative intensities of the experimental structure factors reasonably well over the entire q range. The real-space distances corresponding to the prepeak, $d = 2\pi/q_{max}$, found by experiments and simulations are presented in the inset of Figure 1b. MD simulations slightly overpredict the experimental values; however, the nonmonotonic dependence of the domain distance on composition is well-reproduced. The excellent agreement between MD simulation and experimental results provides confidence in the assignment of certain composition-dependent morphological transitions, which are described by the subsequent detailed analysis of the MD simulations.

The connectivity of the nanosegregated polar/nonpolar structure is examined in a quantitative manner in terms of domain analysis based on the Voronoi tessellation technique.[38] In this analysis, adjacent Voronoi cells sharing a face and belonging to a given subunit constitute a domain. For our purposes, each of the binary ionic liquid mixture systems is characterized in terms of four unique domains: (a) the total polar domain composed of the polar groups of both the cations and the anion; (b) C_8MIm nonpolar; (c) C_2MIm nonpolar; and (d) total nonpolar domain containing the nonpolar groups from both cations. The polar group of both imidazolium cations contains the imidazolium ring as well as the methyl and methylene groups directly bonded to the ring, while the anion is completely polar. The polar group of the cation and anion together constitutes the overall polar domain. The nonpolar regions in the two cations are the respective uncharged carbon groups minus the methylene group directly bonded to the imidazolium ring. The uncharged alkyl chain of the cations is considered unique in order to identify the origin of the structural changes at various concentrations. Figure 2a provides the number of domains based on this classification as a function of the C_2MImBF_4 concentration. As expected, a domain count of 1 is observed for the polar domain, indicating its three-dimensional connectivity for all of the ionic liquid mixtures studied here. This observation is in line with previous simulation studies involving a wide range of pure ionic liquids.[11,15,16,33,38−42] For pure C_2MImBF_4, the domain counts for the nonpolar group are significantly higher than 1 (∼380), indicating that the cation nonpolar groups are dispersed in the system. On the other hand, the domain count for the nonpolar tails in the pure C_8MImBF_4 ionic liquid is between 1 and 2, indicating that the majority of alkyl chains are connected in a single percolated nonpolar domain with some possible occurrence of isolated C_8MImBF_4 nonpolar chains. The addition of 30 mol % C_2MImBF_4 results in a significant disruption of the nonpolar connectivity as the large single continuous domain is broken into as many as 10 separate domains and the number reaches as high as 57 at the highest C_2MImBF_4concentration.

A quantitative metric of the variety of shapes adopted by the polar and nonpolar domains is provided by the isoperimetric quotient, $Q_{peri} = [r_{sphere}(V)/r_{sphere}(A)]^6 = 36\pi[V^2/A^3]$, where V and A denote the volume and area of a given domain,

DOI: 10.1021/acs.jpclett.9b02478
J. Phys. Chem. Lett. 2019, 10, 6274−6280

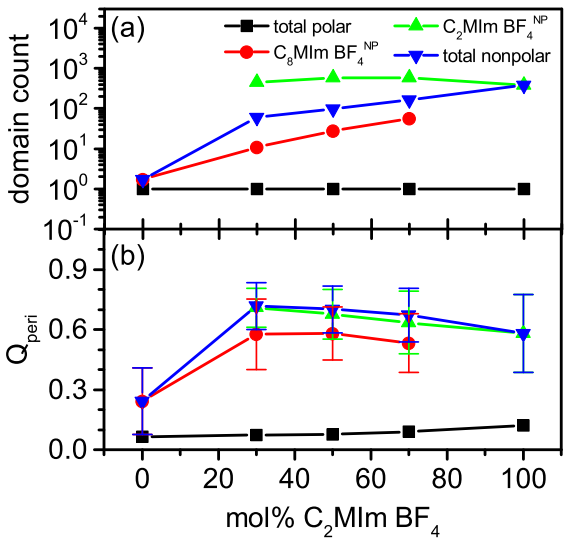

Figure 2. (a) Average domain count of the polar and nonpolar domains present in the simulation box as a function of C_2MImBF_4 concentration. (b) Average isoperimetric quotient, Q_{peri}, of respective cation/anion polar and nonpolar domains as a function of C_2MImBF_4 concentration. Please note that the average numerical value and standard deviations were computed by dividing the trajectory into three blocks.

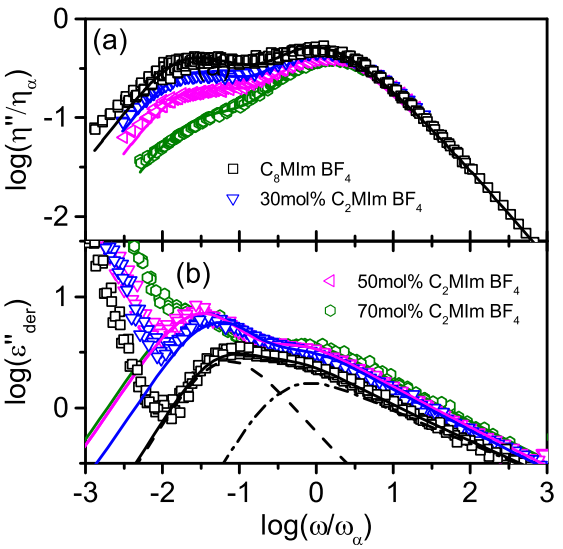

Figure 3. (a) Imaginary part of the complex viscosity, $\eta^* = \eta' - i\eta''$, normalized by the structural relaxation contribution to the zero-shear viscosity, $\eta_\alpha = G_\infty/\omega_\alpha$, versus frequency normalized by the structural relaxation rate, ω_α. Solid lines correspond to the fit by two Cole–Davidson-modified Maxwell relaxation models. (b) Derivative representation of the dielectric loss, ε''_{der}. T = 204–228 K at 8 K increments. Solid lines correspond to the fit of two Havriliak–Negami fit functions at 204 K. The dashed and dotted–dashed lines represent the separate Havriliak–Negami functions of the underlying slow and structural relaxations, respectively, for C_8MImBF_4. Details of the fitting functions are provided in the Supporting Information.

respectively, while $r_{sphere}(V)$ and $r_{sphere}(A)$ represent the equivalent radii of the sphere with volume V and the sphere with area A, respectively. With this definition, the quotient will assume a value of 1 for a perfectly spherical shape, while any deviations from sphericity lead to values lower than 1.[42] The change in the isoperimetric quotient as a function of the C_2MImBF_4 concentration is shown in Figure 2b. From the figure, it is clear that Q_{peri} for the polar domain shows a negligible dependence on the concentration of C_2MImBF_4 and is always less than 0.1, which implies that the shape of the polar network differs greatly from sphericity. Further, the nonpolar domain present in pure C_8MImBF_4 ionic liquid has a Q_{peri} value less than 0.25 and domain count of approximately 1, suggesting a network whose shape is also far from spherical. However, with the introduction of 30 mol % of C_2MImBF_4 in C_8MImBF_4, the Q_{peri} value nearly doubles, assuming a value of ~0.58, suggesting a transition in the morphology of the domains, which now more closely resemble a sphere in comparison to that in the pure C_8MImBF_4. The results are even more dramatic when the total nonpolar domain of the mixture is considered with values approaching as high as 0.7 at 30 mol % C_2MImBF_4. Above 30 mol %, the Q_{peri} is practically composition-independent, indicating that the transition in mesoscale aggregate shape occurs at or below this concentration.

To probe the influence of the composition-dependent morphology on the mesoscale aggregate dynamics, the neat ionic liquids and their mixtures were investigated by dynamic-mechanical and broad-band dielectric spectroscopy. These data are presented in Figure3 in terms of the imaginary part of the complex viscosity, η'', and the derivative representation of the dielectric loss, ε''_{der}, respectively. Two distinct relaxation peaks, well separated in frequency, are observed in each experiment. The rates of the faster, higher-frequency relaxation scale with the calorimetric glass transition temperature, T_g, which follows a weighted average of the two neat IL components. This comparison indicates that in both experiments the faster relaxations arise from the same underlying ion dynamics that define the glass transition.[43,30] By comparison, the slower dielectric relaxation rate, $\omega_{slow,BDS}$, has a more complex composition dependence, as discussed later, indicating that it is not directly associated with the glass transition, as recently suggested.[44] Further details on the T_g's and temperature-dependent relaxation rates are presented in the Supporting Information. In order to emphasize the influence of composition on the slower mesoscale dynamics, the spectra in Figure 3 are shown versus frequency normalized by the rate of the structural relaxation, ω_α.

In neat C_nMImBF_4 ionic liquids, the emergence of the slow dynamics was found to coincide with the onset of solvophobic aggregation, as evidenced by the development of the X-ray scattering prepeak and by a comparison between the relaxation rates with those previously obtained by neutron spin echo spectroscopy.[27,29−31,45,46] Therefore, the slow relaxations were attributed to fluctuations of the mesoscale aggregates at time scales longer than the structural relaxation. This attribution is further substantiated by Yamaguchi's recent computational work, which shows that a cross-correlation exists between the shear stress relaxation and the slow relaxation of the domain structure corresponding to the scattering prepeak.[28] It should also be noted that similar slow, substructural relaxations are also observed in some other mesoscopically ordered liquids, most notably monohydroxy alcohols, where they are also attributed to a supramolecular origin.[47−52] Despite the apparent similarities in the dielectric and dynamic-mechanical spectra, these techniques are sensitive to distinctly different correlations within the bulk liquid, i.e., polarization and the stress tensor, respectively. Therefore, a careful comparison of the influence of composition on the strength and rate of the

DOI: 10.1021/acs.jpclett.9b02478
J. Phys. Chem. Lett. 2019, 10, 6274−6280

slower mesoscale aggregate dynamics, as obtained by each technique, may provide useful insight into its molecular origin.

Upon dilution of C_8MImBF_4 with C_2MImBF_4, the slow mechanical mesoscale relaxation is gradually reduced in strength until at 70 mol % C_2MImBF_4 it is barely visible as a low-frequency shoulder to the structural relaxation. Relative to the structural relaxation rate, the rate of the slow relaxation is independent of composition. This trend is in stark contrast to observations of the slow dielectric relaxation. Upon addition of C_2MImBF_4, the slow dielectric relaxation substantially increases in strength and shifts to lower frequencies relative to the structural, α-relaxation rate. The relaxation rates and strengths are provided in the Supporting Information. The divergence in the composition dependence of the slow relaxations probed by each technique indicates a possible sensitivity of the dielectric relaxation mechanism to the mesoscale aggregate shape or morphology, which is lacking in the mechanical relaxation.

Several factors could potentially influence the mesoscale aggregate dynamics such as the composition-dependent volume fraction, shape, and size of the aggregated nonpolar domains as well as any alteration in ion−ion interactions at the polar/nonpolar interfaces. By our choice of cation and anion for the two ionic liquid components, we have attempted to minimize the latter effect and will not consider it further. The size of the nonpolar domains is probed by the real-space correlation distance corresponding to the X-ray scattering prepeak. These distances, given in the inset of Figure 1b, increase with increasing concentration of C_2MImBF_4. However, the modest increase in aggregate dimensions by ∼2 Å is not considered sufficient to explain the substantial changes in aggregate dynamics observed in the mechanical and dielectric spectra. We also note the relative invariance of the mechanical mesoscale aggregate relaxation rate, as evidence for this relatively minor change in nonpolar domain size. The gradual reduction in the strength of the slow mechanical relaxation is consistent with a reduction in volume fraction of the nonpolar aggregate domains in which it originates. Accordingly, the opposite composition dependence of the slow dielectric relaxation strength suggests an overriding influence of aggregate shape rather than volume fraction.

It is proposed that the slow dielectric relaxation originates from interfacial polarization at the polar/nonpolar interfaces. From numerous studies on heterogeneous liquids and solids, it is well established that interfacial polarizations are strongly dependent on the shapes of the included domains.[53−56] A change in the shapes of the aggregates might therefore be the origin of the observed increases in strength of the slow relaxation. The influence of a transition in aggregate shape on interfacial polarization can be ascertained using an effective medium approximation (EMA). EMAs are useful approximate approaches to relate the shape and volume fractions of a filler phase located within host matrixes to the macroscopic dielectric properties of the composite, provided the properties of the two phases can be estimated.[56−59] Insight into the interplay of aggregate shapes, volume fractions, and dielectric relaxation strengths may be obtained by probing the ability of an EMA to accurately predict the static dielectric permittivities, ε_s, and dc ionic conductivities, σ_0, of the mixtures. These values are defined as the low-frequency limiting values of the real parts of complex dielectric permittivity and complex conductivity, respectively; see the Supporting Information.[58] The static dielectric permittivity, $\varepsilon_s = \Delta\varepsilon_{slow} + \Delta\varepsilon_\alpha + \varepsilon_\infty$, contains contributions from all higher-frequency dielectric relaxations including the structural and slow dielectric relaxation strengths, $\Delta\varepsilon_\alpha$ and $\Delta\varepsilon_{slow}$, as well as other processes included in the high-frequency limiting permittivity, ε_∞. In the ionic liquid mixtures, the composition dependence of ε_s is dominated by and is roughly proportional to the strength of the slow dielectric relaxation. For our investigation, we employ a form of the symmetric Looyenga equation,[57] which is suitable for the conducting phases and intermediate volume fractions found in our IL mixtures.[57] Details of this EMA and our application of it may be found in the Supporting Information. The two fit parameters of this model, n and ϕ, correspond to the shape factor and volume fraction of the nonpolar domain; see Figure 4a. The experimental values of ε_s and σ_0 are predicted only by an increase in n and a concomitant decrease in ϕ. Due to the assumptions on which an evaluation of the EMA relies, these trends can only be interpreted qualitatively. The overall reduction in volume fraction of the nonpolar domain is consistent with its dilution upon addition of the nonaggregating C_2MImBF_4. The shape factor, n, is related to the shape of the insulating phase, with n = 1/3 corresponding to spherical inclusions.[56,57] The gradual increase in n indicates that the increase in ε_s is consistent with a transition in mesoscale aggregate shape.

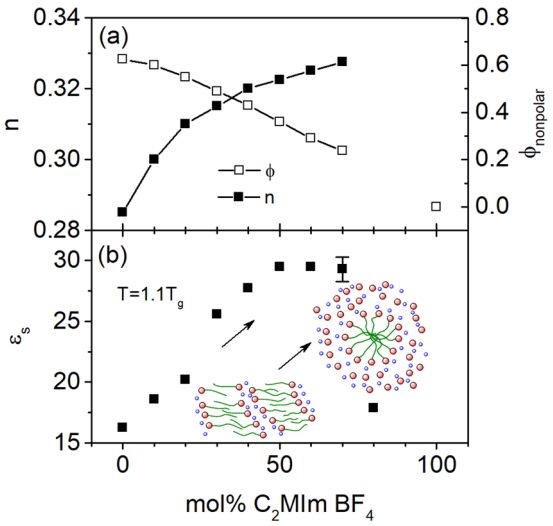

Figure 4. (a) Shape parameter, n, and volume fraction of the nonpolar phase, $\phi_{nonpolar}$, versus mol % C_2MImBF_4. (b) Concentration dependence of static dielectric permittivity at $T = 1.1T_g$. The increase in ε_s is due to the concentration-dependent aggregate shapes illustrated by the inset cartoons.

Due to the close agreement between the trends found by MD simulation, dynamic mechanical spectroscopy, and dielectric spectroscopy, we attribute the increase in ε_s, Figure 4b, and accordingly the strength of the slow dielectric relaxation to a transition in the mesoscale aggregate morphology owing to the dilution of nonpolar domains upon addition of C_2MImBF_4. Together, these results strongly indicate that the slower dielectric relaxation originates in a polarization at the polar/nonpolar interfaces of the mesoscale aggregates. As a direct result of the alteration in mesoscale aggregate morphology, the static dielectric permittivities of the ionic liquid mixtures are increased by almost 100% relative to the neat ionic liquids.

DOI: 10.1021/acs.jpclett.9b02478
J. Phys. Chem. Lett. 2019, 10, 6274−6280

The value of the static dielectric permittivity, ε_s, is commonly linked to the solvating ability of molecular solvents.[60] Literature values of ε_s of aprotic ionic liquids fall around 7−15, typical of low-polarity solvents.[61−64] The substantial increase in ε_s of the ionic liquid mixtures and its direct link to aggregate morphology and dynamics provide a new route to tuning this important physical parameter. Higher ε_s values are expected to influence ionic liquid/solute and ionic liquid/solid-surface interactions, with potentially critical implications for the application of ionic liquids in biomass processing, chemical synthesis, nanoparticle growth, and as electrolytes in solar cells, batteries, and supercapacitors.[1,7,65,66] It should be noted that the actual relation between ε_s and the solvating ability of ionic liquids is an area of open debate. In contrast to nonionic molecular solvents, ionic liquid polarity parameters obtained by solvatochromic studies are often uncoupled from ε_s.[67] Future studies, which further elucidate the influence of mesoscale aggregation and interfacial polarization on ε_s and solvation, may assist in explaining this disparity. More generally, this study highlights the advantage of investigating both mesoscale aggregate morphology and dynamics in order to elucidate the influence of aggregation on the physicochemical properties of ionic liquids.

■ ASSOCIATED CONTENT

Supporting Information

The Supporting Information is available free of charge on the ACS Publications website at DOI: 10.1021/acs.jpclett.9b02478.

Experimental details, simulation details, analysis of the X-ray scattering profiles, DSC results, analysis of the dynamic-mechanical and broad-band dielectric spectra, fit parameters, details of the Looyenga EMA, and details of the MD simulation results (PDF)

■ AUTHOR INFORMATION

Corresponding Authors

*E-mail: jindal.shah@okstate.edu.

*E-mail: jsangoro@utk.edu.

ORCID

Tyler Cosby: 0000-0001-6381-558X

Utkarsh Kapoor: 0000-0002-4977-3405

Jindal K. Shah: 0000-0002-3838-6266

Joshua Sangoro: 0000-0002-5483-9528

Notes

The authors declare no competing financial interest.

■ ACKNOWLEDGMENTS

J.S. acknowledges support by the National Science Foundation, the Division of Chemistry through No. CHE-1753282. T.C. gratefully acknowledges financial support from the U.S. Army Research Office under Contract No. W911NF-17-1-0052. The BDS, DMS, and DSC measurements were conducted at Oak Ridge National Laboratory's Center for Nanophase Materials Sciences, which is sponsored by the Division of Scientific User Facilities, Office of Basic Energy Sciences, U.S. Department of Energy. U.K. and J.K.S. acknowledge support by the National Science Foundation, the Divison of Chemical, Biomolecular, Environmental, and Transport through Grant CBET-1706978. The X-ray scattering experiments were performed at the Duke University Shared Materials Instrumentation Facility (SMIF), a member of the North Carolina Research Triangle Nanotechnology Network (RTNN), which is supported by the National Science Foundation (Grant No. ECCS-1542015) as part of the National Nanotechnology Coordinated Infrastructure (NNCI). The authors extend sincere thanks to Prof. Austen Angell for helpful discussions. Computational resources were provided by the High Performance Computing Cluster at Oklahoma State University.

■ REFERENCES

(1) Hallett, J. P.; Welton, T. Room-Temperature Ionic Liquids: Solvents for Synthesis and Catalysis. 2. *Chem. Rev.* **2011**, *111*, 3508−3576.

(2) He, Z.; Alexandridis, P. Nanoparticles in Ionic Liquids: Interactions and Organization. *Phys. Chem. Chem. Phys.* **2015**, *17*, 18238−18261.

(3) Antonietti, M.; Kuang, D.; Smarsly, B.; Zhou, Y. Ionic Liquids for the Convenient Synthesis of Functional Nanoparticles and Other Inorganic Nanostructures. *Angew. Chem., Int. Ed.* **2004**, *43*, 4988−4992.

(4) MacFarlane, D. R.; Tachikawa, N.; Forsyth, M.; Pringle, J. M.; Howlett, P. C.; Elliott, G. D.; Davis, J. H.; Watanabe, M.; Simon, P.; Angell, C. A. Energy Applications of Ionic Liquids. *Energy Environ. Sci.* **2014**, *7*, 232−250.

(5) Chakrabarti, M. H.; Mjalli, F. S.; AlNashef, I. M.; Hashim, M. A.; Hussain, M. A.; Bahadori, L.; Low, C. T. J. Prospects of Applying Ionic Liquids and Deep Eutectic Solvents for Renewable Energy Storage by Means of Redox Flow Batteries. *Renewable Sustainable Energy Rev.* **2014**, *30*, 254−270.

(6) Smiglak, M.; Pringle, J. M.; Lu, X.; Han, L.; Zhang, S.; Gao, H.; MacFarlane, D. R.; Rogers, R. D. Ionic Liquids for Energy, Materials, and Medicine. *Chem. Commun.* **2014**, *50*, 9228−9250.

(7) Armand, M.; Endres, F.; MacFarlane, D. R.; Ohno, H.; Scrosati, B. Ionic-liquid Materials for the Electrochemical Challenges of the Future. *Nat. Mater.* **2009**, *8*, 621−629.

(8) van Osch, D. J. G. P.; Kollau, L. J. B. M.; van den Bruinhorst, A.; Asikainen, S.; Rocha, M. A. A.; Kroon, M. C. Ionic Liquids and Deep Eutectic Solvents for Lignocellulosic Biomass Fractionation. *Phys. Chem. Chem. Phys.* **2017**, *19*, 2636−2665.

(9) Santos, C. S.; Annapureddy, H. V. R.; Murthy, N. S.; Kashyap, H. K.; Castner, E. W.; Margulis, C. J. Temperature-dependent Structure of Methyltributylammonium bis(trifluoromethylsulfonyl)-amide: X-ray Scattering and Simulations. *J. Chem. Phys.* **2011**, *134*, 064501.

(10) Santos, C. S.; Murthy, N. S.; Baker, G. A.; Castner, E. W. Communication: X-ray Scattering from Ionic Liquids with Pyrrolidinium Cations. *J. Chem. Phys.* **2011**, *134*, 121101.

(11) Hayes, R.; Warr, G. G.; Atkin, R. Structure and Nanostructure in Ionic Liquids. *Chem. Rev.* **2015**, *115*, 6357−6426.

(12) Russina, O.; Lo Celso, F.; Plechkova, N.; Jafta, C. J.; Appetecchi, G. B.; Triolo, A. *Topics in Current Chemistry*; 2017; Vol. *375*; p 58.

(13) Canongia Lopes, J. N. A.; Pádua, A. A. H. Nanostructural Organization in Ionic Liquids. *J. Phys. Chem. B* **2006**, *110*, 3330−3335.

(14) Triolo, A.; Russina, O.; Bleif, H. J.; Di Cola, E. Nanoscale Segregation in Room Temperature Ionic Liquids. *J. Phys. Chem. B* **2007**, *111*, 4641−4644.

(15) Kapoor, U.; Shah, J. K. Globular, Sponge-like to Layer-like Morphological Transition in 1-n-Alkyl-3-methylimidazolium Octylsulfate Ionic Liquid Homologous Series. *J. Phys. Chem. B* **2018**, *122*, 213−228.

(16) Kapoor, U.; Shah, J. K. Effect of Molecular Solvents of Varying Polarity on the Self-Assembly of 1-n-Dodecyl-3-methylimidazolium Octylsulfate Ionic Liquid. *J. Theor. Comput. Chem.* **2018**, *17*, 1840004.

(17) Araque, J. C.; Hettige, J. J.; Margulis, C. J. Modern Room Temperature Ionic Liquids, a Simple Guide to Understanding Their

DOI: 10.1021/acs.jpclett.9b02478
J. Phys. Chem. Lett. 2019, 10, 6274−6280

Structure and How It May Relate to Dynamics. *J. Phys. Chem. B* **2015**, *119*, 12727−12740.
(18) Berrod, Q.; Ferdeghini, F.; Zanotti, J.-M.; Judeinstein, P.; Lairez, D.; García Sakai, V.; Czakkel, O.; Fouquet, P.; Constantin, D. Ionic Liquids: Evidence of the Viscosity Scale-Dependence. *Sci. Rep.* **2017**, *7*, 2241.
(19) Ferdeghini, F.; Berrod, Q.; Zanotti, J.-M.; Judeinstein, P.; Sakai, V. G.; Czakkel, O.; Fouquet, P.; Constantin, D. Nanostructuration of Ionic Liquids: Impact on the Cation Mobility. A Multi-scale Study. *Nanoscale* **2017**, *9*, 1901−1908.
(20) Burankova, T.; Simeoni, G.; Hempelmann, R.; Mora Cardozo, J. F.; Embs, J. P. Dynamic Heterogeneity and Flexibility of the Alkyl Chain in Pyridinium-Based Ionic Liquids. *J. Phys. Chem. B* **2017**, *121*, 240−249.
(21) Aoun, B.; González, M. A.; Ollivier, J.; Russina, M.; Izaola, Z.; Price, D. L.; Saboungi, M.-L. Translational and Reorientational Dynamics of an Imidazolium-Based Ionic Liquid. *J. Phys. Chem. Lett.* **2010**, *1*, 2503−2507.
(22) Griffin, P. J.; Wang, Y.; Holt, A. P.; Sokolov, A. P. Communication: Influence of Nanophase Segregation on Ion Transport in Room Temperature Ionic Liquids. *J. Chem. Phys.* **2016**, *144*, 151104.
(23) Wang, Y.; Voth, G. A. Tail Aggregation and Domain Diffusion in Ionic Liquids. *J. Phys. Chem. B* **2006**, *110*, 18601−18608.
(24) Sonnleitner, T.; Turton, D. A.; Waselikowski, S.; Hunger, J.; Stoppa, A.; Walther, M.; Wynne, K.; Buchner, R. Dynamics of RTILs: A Comparative Dielectric and OKE Study. *J. Mol. Liq.* **2014**, *192*, 19−25.
(25) Turton, D. A.; Hunger, J.; Stoppa, A.; Hefter, G.; Thoman, A.; Walther, M.; Buchner, R.; Wynne, K. Dynamics of Imidazolium Ionic Liquids from a Combined Dielectric Relaxation and Optical Kerr Effect Study: Evidence for Mesoscopic Aggregation. *J. Am. Chem. Soc.* **2009**, *131*, 11140−11146.
(26) Fayer, M. D. Dynamics and Structure of Room Temperature Ionic Liquids. *Chem. Phys. Lett.* **2014**, *616*, 259−274.
(27) Cosby, T.; Vicars, Z.; Wang, Y.; Sangoro, J. Dynamic-Mechanical and Dielectric Evidence of Long-Lived Mesoscale Organization in Ionic Liquids. *J. Phys. Chem. Lett.* **2017**, *8*, 3544−3548.
(28) Yamaguchi, T. Coupling between the Mesoscopic Dynamics and Shear Stress of a Room-temperature Ionic Liquid. *Phys. Chem. Chem. Phys.* **2018**, *20*, 17809−17817.
(29) Russina, O.; Lo Celso, F.; Plechkova, N. V.; Triolo, A. Emerging Evidences of Mesoscopic-Scale Complexity in Neat Ionic Liquids and Their Mixtures. *J. Phys. Chem. Lett.* **2017**, *8*, 1197−1204.
(30) Russina, O.; Beiner, M.; Pappas, C.; Russina, M.; Arrighi, V.; Unruh, T.; Mullan, C. L.; Hardacre, C.; Triolo, A. Temperature Dependence of the Primary Relaxation in 1-Hexyl-3-methylimidazolium bis{(trifluoromethyl)sulfonyl}imide. *J. Phys. Chem. B* **2009**, *113*, 8469−8474.
(31) Kofu, M.; Nagao, M.; Ueki, T.; Kitazawa, Y.; Nakamura, Y.; Sawamura, S.; Watanabe, M.; Yamamuro, O. Heterogeneous Slow Dynamics of Imidazolium-Based Ionic Liquids Studied by Neutron Spin Echo. *J. Phys. Chem. B* **2013**, *117*, 2773−2781.
(32) Castner, E. W.; Wishart, J. F. Spotlight on Ionic Liquids. *J. Chem. Phys.* **2010**, *132*, 120901.
(33) Shimizu, K.; Bernardes, C. E. S.; Canongia Lopes, J. N. Structure and Aggregation in the 1-Alkyl-3-Methylimidazolium Bis(trifluoromethylsulfonyl)imide Ionic Liquid Homologous Series. *J. Phys. Chem. B* **2014**, *118*, 567−576.
(34) Shimizu, K.; Costa Gomes, M. F.; Pádua, A. A. H.; Rebelo, L. P. N.; Canongia Lopes, J. N. Three Commentaries on the Nano-Segregated Structure of Ionic Liquids. *J. Mol. Struct.: THEOCHEM* **2010**, *946*, 70−76.
(35) Teubner, M.; Strey, R. Origin of the Scattering Peak in Microemulsions. *J. Chem. Phys.* **1987**, *87*, 3195.
(36) Weiss, H.; Mars, J.; Li, H.; Kircher, G.; Ivanova, O.; Feoktystov, A.; Soltwedel, O.; Bier, M.; Mezger, M. Mesoscopic Correlation Functions in Heterogeneous Ionic Liquids. *J. Phys. Chem. B* **2017**, *121*, 620−629.
(37) Bruce, D. W.; Cabry, C. P.; Canongia Lopes, J. N.; Costen, M. L.; D'Andrea, L.; Grillo, I.; Marshall, B. C.; McKendrick, K. G.; Minton, T. K.; Purcell, S. M.; et al. Nanosegregation and Structuring in the Bulk and at the Surface of Ionic-Liquid Mixtures. *J. Phys. Chem. B* **2017**, *121*, 6002−6020.
(38) Brehm, M.; Kirchner, B. TRAVIS - A Free Analyzer and Visualizer for Monte Carlo and Molecular Dynamics Trajectories. *J. Chem. Inf. Model.* **2011**, *51*, 2007−2023.
(39) Bernardes, C. E. S.; Shimizu, K.; Lobo Ferreira, A. I. M. C.; Santos, L. M. N. B. F.; Canongia Lopes, J. N. Structure and Aggregation in the 1,3-Dialkyl-imidazolium Bis-(trifluoromethylsulfonyl)imide Ionic Liquid Family: 2. From Single to Double Long Alkyl Side Chains. *J. Phys. Chem. B* **2014**, *118*, 6885−6895.
(40) Shimizu, K.; Canongia Lopes, J. N. Probing the Structural Features of the 1-alkyl-3-methylimidazolium Hexafluorophosphate Ionic Liquid Series Using Molecular Dynamics Simulations. *J. Mol. Liq.* **2015**, *210*, 257−263.
(41) Shimizu, K.; Freitas, A. A.; Canongia Lopes, J. N. Structural Characterization of the [CnC1im][C4F9SO3] Ionic Liquid Series: Alkyl Versus Perfluoroalkyl Side Chains. *J. Mol. Liq.* **2017**, *226*, 28−34.
(42) Brehm, M.; Weber, H.; Thomas, M.; Hollóczki, O.; Kirchner, B. Domain Analysis in Nanostructured Liquids: A Post-Molecular Dynamics Study at the Example of Ionic Liquids. *ChemPhysChem* **2015**, *16*, 3271−3277.
(43) Sangoro, J. R.; Kremer, F. Charge Transport and Glassy Dynamics in Ionic Liquids. *Acc. Chem. Res.* **2012**, *45*, 525−532.
(44) Pabst, F.; Gabriel, J.; Blochowicz, T. Mesoscale Aggregates and Dynamic Asymmetry in Ionic Liquids: Evidence from Depolarized Dynamic Light Scattering. *J. Phys. Chem. Lett.* **2019**, *10*, 2130−2134.
(45) Cosby, T.; Vicars, Z.; Heres, M.; Tsunashima, K.; Sangoro, J. Dynamic and Structural Evidence of Mesoscopic Aggregation in Phosphonium Ionic Liquids. *J. Chem. Phys.* **2018**, *148*, 193815.
(46) Griffin, P. J.; Holt, A. P.; Tsunashima, K.; Sangoro, J. R.; Kremer, F.; Sokolov, A. P. Ion Transport and Structural Dynamics in Homologous Ammonium and Phosphonium-based Room Temperature Ionic Liquids. *J. Chem. Phys.* **2015**, *142*, 084501.
(47) Gainaru, C.; Wikarek, M.; Pawlus, S.; Paluch, M.; Figuli, R.; Wilhelm, M.; Hecksher, T.; Jakobsen, B.; Dyre, J. C.; Böhmer, R. Oscillatory Shear and High-pressure Dielectric Study of 5-methyl-3-heptanol. *Colloid Polym. Sci.* **2014**, *292*, 1913−1921.
(48) Hecksher, T.; Jakobsen, B. Communication: Supramolecular Structures in Monohydroxy Alcohols: Insights from Shear-mechanical Studies of a Systematic Series of Octanol Structural Isomers. *J. Chem. Phys.* **2014**, *141*, 101104.
(49) Hecksher, T. Communication: Linking the Dielectric Debye Process in Mono-alcohols to Density Fluctuations. *J. Chem. Phys.* **2016**, *144*, 161103.
(50) Arrese-Igor, S.; Alegría, A.; Colmenero, J. Multimodal Character of Shear Viscosity Response in Hydrogen Bonded Liquids. *Phys. Chem. Chem. Phys.* **2018**, *20*, 27758−27765.
(51) Böhmer, R.; Gainaru, C.; Richert, R. Structure and Dynamics of Monohydroxy Alcohols-Milestones Towards Their Microscopic Understanding, 100 Years after Debye. *Phys. Rep.* **2014**, *545*, 125−195.
(52) Yamaguchi, T.; Saito, M.; Yoshida, K.; Yamaguchi, T.; Yoda, Y.; Seto, M. Structural Relaxation and Viscoelasticity of a Higher Alcohol with Mesoscopic Structure. *J. Phys. Chem. Lett.* **2018**, *9*, 298−301.
(53) Torquato, S. *Random Heterogeneous Materials: Microstructure and Macroscopic Properties*; Springer-Verlag: New York, 2002; p 701.
(54) Choy, T. C. *Effective Medium Theory*; Oxford University Press: New York, 1999; p 200.
(55) Looyenga, H. Dielectric Constants of Heterogeneous Mixtures. *Physica* **1965**, *31*, 401−406.
(56) van Beek, L. K. H. In *Progress in Dielectrics*; Birks, J. B., Ed.; Heywood Books: London, 1967; Vol. 7.

DOI: 10.1021/acs.jpclett.9b02478
J. Phys. Chem. Lett. 2019, 10, 6274−6280

(57) Boyle, M. H. The Electrical-Properties of Heterogeneous Mixtures Containing an Oriented Spheroidal Dispersed Phase. *Colloid Polym. Sci.* **1985**, *263*, 51−57.
(58) Kremer, F.; Schönhals, A. *Broadband Dielectric Spectroscopy*; Springer: Berlin, 2003; p 729.
(59) Mizoshiri, M.; Nagao, T.; Mizoguchi, Y.; Yao, M. Dielectric Permittivity of Room Temperature Ionic Liquids: A Relation to the Polar and Nonpolar Domain Structures. *J. Chem. Phys.* **2010**, *132*, 164510.
(60) Reichardt, C.; Welton, T. *Solvents and Solvent Effects in Organic Chemistry*, 4th ed.; Wiley-VCH, 2010; p 692.
(61) Weingärtner, H. The Static Dielectric Permittivity of Ionic Liquids. *J. Mol. Liq.* **2014**, *192*, 185−190.
(62) Huang, M.-M.; Jiang, Y.; Sasisanker, P.; Driver, G. W.; Weingärtner, H. Static Relative Dielectric Permittivities of Ionic Liquids at 25°C. *J. Chem. Eng. Data* **2011**, *56*, 1494−1499.
(63) Weingärtner, H. Understanding Ionic Liquids at the Molecular Level: Facts, Problems, and Controversies. *Angew. Chem., Int. Ed.* **2008**, *47*, 654−670.
(64) Wakai, C.; Oleinikova, A.; Ott, M.; Weingärtner, H. How Polar are Ionic Liquids? Determination of the Static Dielectric Constant of an Imidazolium-based Ionic Liquid by Microwave Dielectric Spectroscopy. *J. Phys. Chem. B* **2005**, *109*, 17028−17030.
(65) Kim, T.; Chang Kang, H.; Thanh Tung, T.; Don Lee, J.; Kim, H.; Seok Yang, W.; Gyu Yoon, H.; Suh, K. S. Ionic Liquid-assisted Microwave Reduction of Graphite Oxide for Supercapacitors. *RSC Adv.* **2012**, *2*, 8808−8812.
(66) Fedorov, M. V.; Kornyshev, A. A. Ionic Liquids at Electrified Interfaces. *Chem. Rev.* **2014**, *114*, 2978−3036.
(67) Baker, G. A.; Rachford, A. A.; Castellano, F. N.; Baker, S. N. Ranking Solvent Interactions and Dielectric Constants with Pt(mesBIAN)(tda): A Cautionary Tale for Polarity Determinations in Ionic Liquids. *ChemPhysChem* **2013**, *14*, 1025−1030.

DOI: 10.1021/acs.jpclett.9b02478
J. Phys. Chem. Lett. 2019, 10, 6274−6280